Title

The Vibration Behavior of Sub-Micrometer Gas Vesicles in Response to Acoustic Excitation Determined via Laser Doppler Vibrometry

Journal

Advanced Functional Materials, 30(13)

ISSN

1616-301X

Authors

Zhang, Shuai
Huang, An
Bar-Zion, Avinoam
et al.

Publication Date

2020-03-01

DOI

10.1002/adfm.202000239

Peer reviewed

The vibration behavior of submicron gas vesicles in response to acoustic excitation determined via laser Doppler vibrometry

Shuai Zhang,[†,⊥] An Huang,[†,⊥] Avinoam Bar-Zion,[‡] Jiaying Wang,[¶] Oscar Vazquez Mena,[¶] Mikhail G. Shapiro,[‡] and James Friend[*,§,‖]

†*Medically Advanced Devices Laboratory, Department of Materials Science and Engineering, University of California San Diego, La Jolla, CA, 92093, United States*

‡*Division of Chemistry and Chemical Engineering, California Institute of Technology, Pasadena, CA, 91125, United States*

¶*Medically Advanced Devices Laboratory, Department of Nanoengineering, University of California San Diego, La Jolla, CA, 92093, United States*

§*Medically Advanced Devices Laboratory, Departments of Mechanical and Aerospace Engineering and Materials Engineering, University of California San Diego, La Jolla, CA, 92093, United States*

‖*Medically Advanced Devices Laboratory, Department of Surgery, School of Medicine, University of California San Diego, La Jolla, CA, 92093, United States*

⊥*These authors contributed equally to this work.*

E-mail: jfriend@eng.ucsd.edu

Abstract

We report the ability to monitor submicron gas vesicles' vibration behavior to nonlinear buckling and collapse using laser Doppler vibrometry, providing a precise non-contact

technique for monitoring the motion of submicron objects. The fundamental and first harmonic resonance frequencies of the vesicles were found to be 1.024 GHz and 1.710 GHz, respectively. An interparticle resonance was furthermore identified at approximately 300 MHz, inversely dependent upon the agglomerated GV size of around 615 nm. Most importantly, the vesicles amplify and broaden input acoustic signals at far lower frequencies—for example, 7 MHz—associated with medical and industrial applications, and they were found to transition from a linear to nonlinear response at 150 kPa and to collapse at 350 kPa or greater.

Introduction

Microbubbles, made stable through tailored coatings, are useful across many disciplines—especially in medicine, pharmacology, materials science, food engineering, and water treatment.[1–3] They have long been[1] injected into humans and animals alike for ultrasound imaging as a contrast agent,[4] exploiting their significant contrast difference with the surrounding tissue and their safe dissolution and resorption after a few minutes. When functionalized, they are especially useful for delivering drugs and genetic material and serving as cavitation nucleation sites for disrupting tumor cells.[5]

Researchers are exploring ultrasound imaging into interstitial regions and across vessel walls in tumors where traditional microbubbles are too large to penetrate, driving interest in submicron to nanoscale bubbles.[6] Moreover, reducing the bubble size increases their number density for the same total bubble volume, improving the resolution and specificity of multimodal imaging and therapeutic applications.[7]

Bubbles of whatever scale are known to oscillate in response to incident ultrasound pressure waves, scattering the ultrasound through the surrounding medium. Ultrasound contrast-aided imaging relies upon the detection of nonlinear signals from the bubbles that arise when the oscillation amplitudes become large,[1] and the details of micro-sized bubble oscillation have and continue to be theoretically and experimentally studied.[8] Because bubbles are multi-phase sys-

tems, with a gas surrounded by liquid and perhaps a third media as the coating at the interface to stabilize the gas, any analysis should first be divided into free and coated bubble treatments, producing a significant difference in the complexity of the analysis.[9] For free bubbles, the contained gas is directly in contact with the liquid surrounding it. However, the Laplace pressure is sufficient to require a stabilizing coating on submicron to nano-scale bubbles to avoid their premature resorption.[1]

Gas vesicles (GVs) are a family of gas-filled protein nano-sized structures naturally expressed by photosynthetic microbes as a means to achieve buoyancy in water,[10–13] offering a number of advantages peculiar to their small size and characteristics. The potential benefits of purified nano-scale GVs include ultrasonic imaging to unprecedentedly tiny regions of vasculature and the interstitial space within tumors.[14–16] Recently introduced acoustic reporter gene cassettes can be used for the imaging of gene expression into deep tissue, through conditional production of GVs in engineered bacteria[17] and mammalian cells.[15] Despite the free diffusion of gas through them, the GVs' amphiphilic shells make them physically stable for long periods of time—weeks to months—both within these microbes and without. They can withstand external pressures of hundreds of kilopascals without collapsing. Further, the GVs can self-assemble into long-range ordered structures without external application of any forces.[18]

While GVs offer many advantages due to their small size, because they are so small, their vibrations under ultrasound stimulation are difficult to observe using light microscopy and consequently remain poorly understood.[19]

In order to most effectively use ultrasound with bubbles, researchers have adopted imaging methods from high frame-rate microscopic imaging[20–23] to the transmission and reception of ultrasound via transducers to determine the intensity of the scattered ultrasound signal. This signal is then correlated to models of the bubbles' vibration behaviors. While the transmitters in most studies are similar, different receivers are used depending on the circumstances, including paired transmitting/receiving ultrasonic transducers[8,24,25] and laser Doppler vibrometers (LDV).[26] Although the LDV has been reported to generate results consistent with high-speed

imaging in measuring the vibration of micro-scale objects, it has so far not been used in any observation of the vibration of *submicron* objects.[27]

Most importantly, the vibration modes of GVs have not yet been directly observed.[28] Furthermore, the resonance frequencies of the GV are unknown but are expected to be greater than microbubbles—which exhibit resonances in the megahertz range—and potentially could reach gigahertz frequencies. In addition, numerical models predict GV buckling across a wide range of ultrasound pressure levels, producing strong nonlinear signals theorized to be due to the buckling;[28] though the nonlinearity has been observed, the buckling has not.

In this paper, we propose to use laser Doppler vibrometry to observe the GVs' vibration behavior. Unlike widely used techniques for understanding microbubble vibration that fail at the submicron scales of GVs and frequencies beyond a few MHz, LDV employs interferometry, offering far better spatiotemporal resolution of up to 2.4 GHz in frequency and for motions as little as 200 fm.[29] However, we must agglomerate the GVs to a size greater than the wavelength of the laser used in the LDV, in our case 532 nm, in order to make them observable. We further must pin the GVs to a surface to enable reliable LDV observation. Using analysis borne from theoretical models and computations, we show how these acts only weakly affect the experimentally observed resonant *frequencies* of the GVs,* with a fundamental resonance at 1 GHz and the first harmonic at 1.7 GHz. In agglomerating the GVs to ~615 nm, we identify the existence of a new vibration mode from the entire agglomeration at ~300 MHz. Finally, we elucidate the GVs' responses to a controlled, acoustically-delivered pressure at a clinically-relevant 7 MHz, representing excitation well away from their individual and agglomerate resonances, all the way to buckling and collapse. To our knowledge, this is the first time that the vibration behavior of nano-sized GVs have been directly measured, and furthermore the first time that an LDV has been used to measure the motion of nano-scale objects.

*Though they do significantly affect the resonant mode shapes, as shown in the Supplementary Information.

Results and Discussion

Resonant response of GVs

Using the LDV to measure the vibration of agglomerated avidin-biotin-bound GVs as later described in the methods section and shown in Fig. 1, we identified two well-defined Lorentzian[30] resonance responses centered at 1.025 GHz (Fig. 1(e)) and 1.71 GHz (Fig. 1(h)) that appear from linear response to excitation from the transducer: the measured frequency corresponds to the excitation frequency over the frequency range of the plots. These responses represent a physical motion of the GVs, as the motion of the gold substrate in their absence (Fig. 1(f,i)) lacks these responses, and other aspects of the experiment are controlled to maintain identical conditions.

Consequently, we next consider whether these motions represent individual GV vibration, and whether the motions correspond to coated bubbles where the coating acts to reinforce the bubble's rigidity. We employ a theoretical model[31] derived to determine such bubbles' resonance frequencies,

$$f_s^2 = \frac{3}{\rho_l R^2} K_\nu. \tag{1}$$

Here the compressibility is $K_\nu = \kappa P + \frac{4}{3}\frac{\chi}{R}$, where χ is the elastic compression modulus and $\kappa \approx 1$ is the polytropic exponent. By comparison, the compressibility of non-coated, free bubbles is instead $K_\nu = \kappa P + \frac{3\kappa-1}{3}\frac{2\sigma_w}{R}$ with σ_w as the surface tension between water and air. Here, we equate the model's spherical volume to the volume of the allantoid GVs' volume to give $R^2 = 1.69 \times 10^{-14}$ m^2 for the radius of the sphere, squared, and $\rho_l \sim 1000$ kg/m^3 and $K_\nu \sim 10^7$ Pa,[32] producing a fundamental resonance frequency of $\sim 10^9$ Hz.[†] This result is a similar order of magnitude to the resonance frequencies observed in our experiments. Damping is omitted as $ka \ll 1$, and doing so substantially simplifies the analysis. The prediction from these equations for the resonance of the ~ 615 nm GV *agglomeration* is much lower, an order of magnitude of

[†]The actual estimate from eqn. (1) is about 1.5 GHz, but this prediction presumes the objects are spherical, and the GVs are allantoid. The analysis is therefore used to solely *estimate* the order of magnitude of the resonance frequencies. For the spherical bubbles to specifically produce a 1 GHz resonance, they would need to have a diameter of approximately 240 nm.

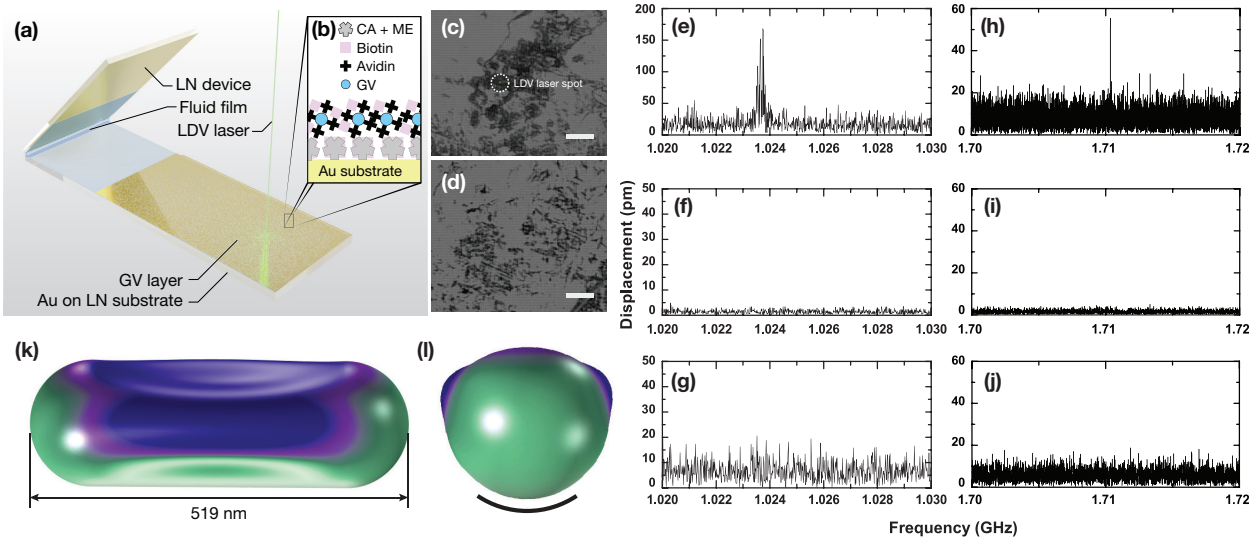

Figure 1: The (a) LN transducer is coupled via a thin fluid film spread across a second gold-LN substrate with a 45° angle between them. This arrangement ensures effective acoustic wave transmission into the fluid film while avoiding occlusion of the LDV. The avidin-conjugated GVs are (b) bound to the gold substrate via biotin and CA+ME. Transmitted light microscopy of the as-bound GVs indicates (c) intact GVs, and (d) collapsed GVs after exposure to intense (330 kPa) harmonic acoustic pressure at 6.5 MHz (c,d: scale bars are 20 μm), the fundamental thickness-mode resonance frequency of the LN transducer. Ten trials were conducted, and these results were indistinguishable to the resolution of the LDV. The green dot in (c) represents the size of the LDV laser measurement spot used to produce the (e-j) LDV spectra using an acoustic pressure of 38 kPa. A (e) fundamental linear resonance peak appears at 1.025 GHz only in the presence of the GVs; it is absent with (f) only the gold substrate and (g) after the GVs have been collapsed using an acoustic pressure of 400 kPa at 6.5 MHz. No response peak exists for the GVs below this frequency, except for a response at ~300 MHz discussed later. The next resonance peak to appear, the first harmonic, is (h) at 1.71 GHz with GVs, and is once again absent with (i) only the gold substrate or (j) the GVs after their collapse. These results are of the same order as predictions from the modified Rayleigh-Plesset equation (*see* text) and closely correspond to the predicted fundamental resonance frequency, 1.09 GHz, from computational analysis. The corresponding ((k) side view and (l) end view) fundamental resonance mode shape is provided for a 519 nm-long, 140 nm radius GV, taking into account both the fluid loading and the surface binding as explained in the methods. The heavy curved line indicates the region of binding in the (l) end view.

100 MHz, and in fact a separate resonance of the GV agglomerations appears at ~ 300 MHz as discussed later.

In the past, the resonance frequency of GVs has been posited to be anywhere from a few kilohertz to a few megahertz,[14] and, compared to these estimates, our results here rather closely correspond to our experimental observations. The correspondence also indicates the GV is a nano-sized bubble coated with a significant elastic membrane. Treating them otherwise, as explained in detail in the Supplemental Information, produces flawed resonance frequency predictions.

As hollow structures with significant elastic shells, it should be possible to collapse the GVs with sufficient acoustic pressure, and the collapse may be permanent. Figure 1(g,j) shows that after applying 400 kPa at 6.5 MHz, the resonance frequency of our transducer, LDV measurements of the exposed GVs around 1.025 and 1.71 GHz have disappeared. Only noise remains, a consequence of the poorer reflectivity of the GVs, and otherwise resembling the response of the gold substrate alone (Fig. 1(f,i)). The disappearance of the signal may come from the collapse of the GVs, later considered in detail.

In seeking to better understand the effects of surface binding and agglomeration, we conducted computations to estimate the resonance frequencies and mode shapes of individual fluid-loaded and surface-bound GVs corresponding to those used in the experiments. The fundamental resonance of individual, surface-bound unagglomerated GVs is predicted by computation to be 1.047 GHz, within 0.9% of the experimentally measured (1.025 GHz) value, and producing a mode shape as illustrated in Fig. 1(k,l). Remarkably, agglomerating or binding the GVs only weakly affect their resonance frequencies (*compare* Suppl. Figs. S3 to S5), from a frequency of 0.992 GHz for an individual GV when completely free to 1.09 GHz when bound to a surface as an individual GV and 1.06 GHz when bound and agglomerated to another two GVs—representing the more general case. While this may seem peculiar, it is important to keep in mind that the volume of entrapped gas remains fixed despite these changes in the binding, and consequently the resonance *frequencies* described in large part by the oscillation of those gas

bubbles should not be expected to drastically change. However, it is equally important to note that the resonance *shapes* are predicted by computation to be strongly affected by the binding, an aspect difficult to measure via LDV or another method.

There is another curious phenomena. While the minor diameter of the GV is generally constant, its length can vary depending on growth time and conditions, from a sphere to a long allantoid.[19] We knew a diversity of GVs was present in our samples, yet the resonant response was consistently well-defined and invariant. As indicated from Supplemental Fig. S3, the effect of varying the length of the GV only weakly affects the resonant response. Specifically, the change in the fundamental resonance frequency f with respect to GV length, L, is $df/dL = 0.002$ GHz/nm for $494 \leq L \leq 544$ nm, and so this is why we see a consistent set of resonances throughout (*see* Suppl. Fig. S4).

Resonant response of GV agglomerates

At frequencies significantly lower than the resonance frequencies of the individual GVs, the sole significant response from the system beyond 6.5 MHz is a small but prominent response peak at around 300 MHz. The peak has a maximum displacement of about 18 pm (*see* Fig. 2(b)) in linear response to a narrowband 38 kPa sweep excitation from 300 to 400 MHz. This peak is only present with GVs: the biotin-treated gold substrate shows no such response in Fig. 2(a), and the response peak disappears as shown in Fig. 2(c) after exposure to 400 kPa, 6.5 MHz acoustic waves that appear to collapse the GVs.

The mechanism responsible for these 300 MHz peaks (Fig. 2(b)) may be the resonant vibration of the GV agglomerates as a whole. The measured vibration responses obtained here are broader and weaker than the individual GV resonant responses observed at 1 GHz and beyond (Fig. 1(e,h)). Furthermore, the response frequencies at around 300 MHz can vary from experiment to experiment between 280 to 320 MHz (*see* Suppl. Fig. 2), unlike the nearly identical results obtained for the resonances of the individual GVs.

The slight variation in observed resonance frequencies—from 280 to 320 MHz, as shown in

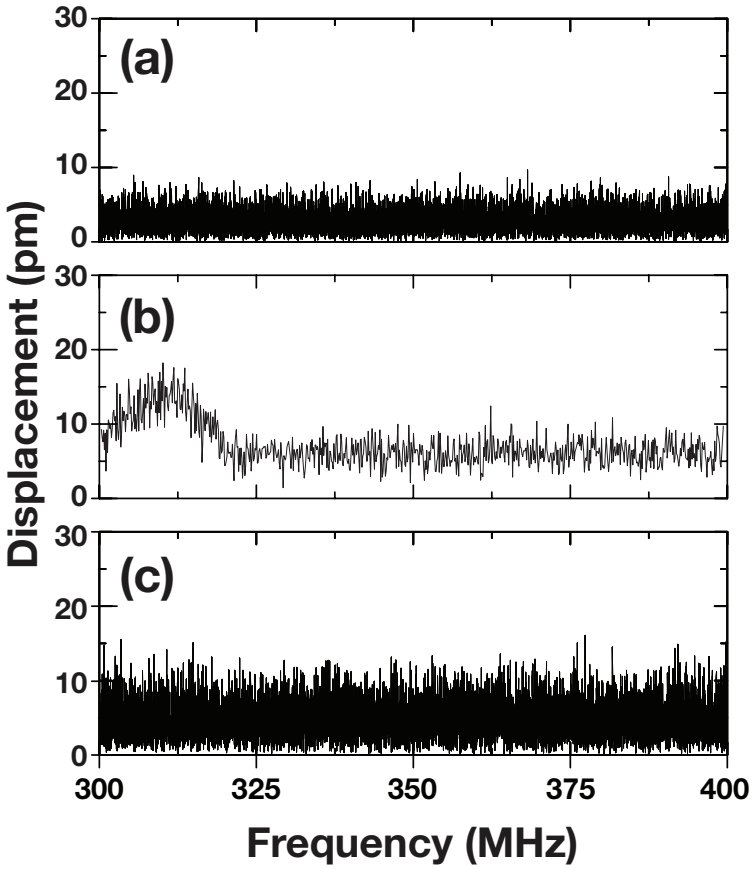

Figure 2: The LDV-measured displacement response from 300 to 400 MHz from narrowband driven vibration at 38 kPa for (a) a biotin-coated gold substrate without GV agglomerates, and (b) GV agglomerates upon the gold substrate. After exposure to 400 kPa at 6.5 MHz, a return to measure the response of the (c) GV agglomerates to 38 kPa from narrowband-driven vibration from 300 to 400 MHz shows the response has disappeared, likely indicating the GVs' collapse.

Suppl. Fig. S6—is correlated with a measured variation in the size of the GV agglomerates, 589 to 640 nm. If we treat the agglomeration as a collection of cavities with a known void fraction, U, we may calculate[33] the collective resonance frequency, $f_U = (2\pi R)^{-1}\sqrt{3\gamma P/\rho U}$, where P is the static pressure within a gas-filled structure in the absence of the ultrasound, and the ratio of specific heats $\gamma = 1$. If we assume the aggregated structure size is 615 nm as provided from our dynamic light measurements, the presumption that $f_U = 300$ MHz then produces[34] a void fraction $U = 3\gamma P/\left[\rho\left(2\pi R f_U\right)^2\right] \sim 10^{-4}$, a reasonable value. If we then use $U \sim 10^{-4}$ as the void fraction for our GV agglomerates, the range of observed agglomerate sizes in our study of 589 to 640 nm produces a commensurate shift in f_U from 313 to 289 MHz, reasonably similar to the observed range of these GV agglomerates' resonance frequencies, 280–320 MHz.

Vibration response of GVs to medically relevant ultrasound

We next examine the GVs response to lower frequency acoustic sources typical in medical imaging, as they are anticipated to be especially useful as ultrasound contrast media. The GVs act to *nonresonantly* amplify the response from ultrasound at 6.5 MHz as shown in Fig. 3(a,b), though the response is also observed to be broader and noisier with GVs (Fig. 3(a)) than without (Fig. 3(b)). The increase in noise is likely from the LDV measurement: the intensity of the specularly reflected laser light from the GVs is significantly less than from the gold substrate, leading to a noisier result in this and the previous LDV results when GVs are present.

To quantify the nonresonant amplification of ultrasound from the presence of the GVs, we used the Rayleigh-Plesset equation to represent the vibration behavior of the bubbles, modified to take into account the presence of the elastic shell. The original Rayleigh-Plesset model[35] relies upon the Rayleigh equation[36] to describe the vibration of free uncoated bubbles with only surface tension, the viscosity of the surrounding liquid, and pressure as a function of time into consideration, producing

$$\rho R\ddot{R} + \frac{3}{2}\rho\dot{R}^2 = p_i - p_{\text{atm}} - \frac{2\sigma}{R} - \frac{4\mu}{R}\dot{R}, \tag{2}$$

where ρ is the density of the liquid surrounding the bubbles, p_{atm} is the ambient pressure, and μ is the viscosity of the fluid. To incorporate the shell structure of the GV, the pressure expression on the right-hand side of eqn. (2) needs to be modified to produce[32]

$$\rho_l\left(R\ddot{R}+\frac{3}{2}\dot{R}^2\right)=p_{\text{atm}}\left[\left(1-\frac{3\kappa\dot{R}}{c}\right)\left(\frac{R_0}{R}\right)^{3n}-1\right]-p_s(R)-\frac{R}{c}\dot{p}_s(R)$$
$$-p_L(R)-\frac{R}{c}\dot{p}_L(R)-\frac{4\mu\dot{R}}{R}-\frac{4\mu R}{c}\left(\frac{\ddot{R}}{R}-\frac{\dot{R}^2}{R^2}\right)-p_h-P_a(t), \tag{3}$$

where R, $\dot{R}$, and $\ddot{R}$ are the GV's radius and its derivatives, and R_0 is its equilibrium radius. In addition to the ambient pressure p_{atm} and hydrostatic pressure p_h, the effects of pressure differential p_s and Laplace pressure caused by shell-liquid interfacial tension p_L are taken into account, and μ is the viscosity of the surrounding liquid. The speed of sound in the surrounding liquid is c, the polytropic index $\kappa = 1.4$ for a perfect gas, and p_a is the acoustic pressure. The acoustic pressure applied to the GVs is difficult to measure and thus we estimated it from the vibration amplitude in Fig. 3(b) of the gold surface the GVs are directly bonded to. The acoustic pressure is determined from first principles as $p_a = \rho_s c^2 k\delta$ with ρ_s as the density of LN (as the gold is a very thin layer and therefore mechanically insignificant here), k the wavenumber, and δ the displacement amplitude of the gold surface. In our case, $\rho_s = 4650\ \text{kg/m}^2$, $k = \frac{2\pi f}{c} = 6.28\times10^3\ \text{m}^{-1}$ and $c = 6.6\times10^3$ m/s. To overcome the effects of noise in Fig. 3(b), we least-squares fitted the data to a Lorentzian function and used the result to complete our calculations via the Rayleigh-Plesset equation, indicated in Fig. 3(a) in comparison to the experimental results. It can be seen from Fig. 3(a) that prediction of displacement of GVs with Rayleigh-Plesset model is larger than the LDV measurements. This discrepancy is not surprising given the spherical bubbles assumed in the model and allantoid GVs in reality, though the results are of a similar order of magnitude.

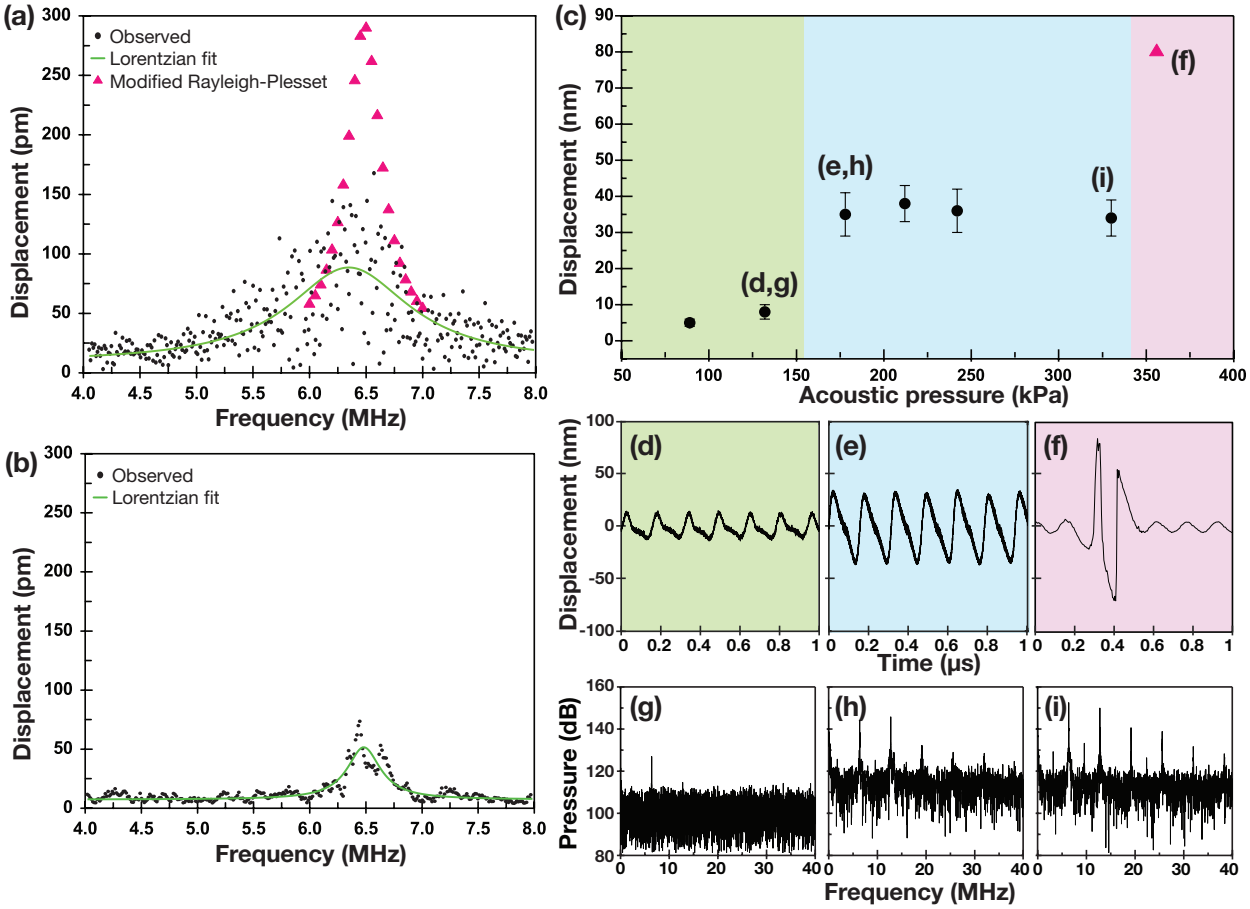

Figure 3: The frequency response of the GVs from 4.0 to 8.0 MHz to 38 kPa acoustic pressure oscillations (a) on the gold substrate is both larger and broader than (b) the gold substrate alone as measured using an LDV. Using the Rayleigh-Plesset equation with modifications by Cherin to accommodate the presence of the elastic shell, the (a) amplitude of the vibration is predicted to be 160 pm, larger than but comparable to the experimental results. The (a,b) fitted data is a least-squares fit to a Lorentzian response typical of a linear resonant dynamic system. The maximum peak height of the curve in (a) is 77.54 pm and in (b) it is 54.07 pm. The half-peak widths for the fitted curves in (a,b) are 1.4471 MHz and 0.397 MHz respectively. The (c) vibration response of the GVs to 6.5 MHz large amplitude excitation shows that, as the acoustic pressure is increased, the LDV-measured displacement of the GVs grows nonlinearly, with three key regions. The GV response to (d) relatively low-pressure excitation is typical of bubble vibration responses over time. Upon (e) increasing the amplitude of the excitation pressure, the GV displacement plateaus at about 40 nm, showing (e) the characteristic sawtooth response of bubbles nearing buckling. Upon exceeding 3.5 MPa excitation pressure, the (c) amplitude of the GV vibration is nearly doubled, but (f) only for a single cycle, after which the response is far lower than even for the (c,d) low-pressure excitation. The error bars represent the range of GV vibration amplitude over 1000 cycles. The frequency spectra of the GVs' radiated sound pressure due to an oscillatory excitation pressure of (g) 132 kPa, (h) 178 kPa and (i) 330 kPa, respectively, shows the appearance of a (g) linear response in the green region, followed by (h) standard harmonics due to finite amplitude deformation and (i) a subharmonic and superharmonics indicating nonlinear coupling in the system.

The buckling and collapse of GVs

Buckling is a particularly interesting nonlinear phenomenon with coated bubbles, and appears upon driving large oscillations in or upon applying large forces to the bubbles. When oscillations are small, it is known[37] that the bubble exhibits radial oscillations and the bubble coating is subjected to significant in-plane stresses that, with growth in the oscillation amplitude, begin to exhibit a non-linear response that becomes non-uniform over the bubble surface and leads to buckling.

To obtain sufficient acoustic pressure from our system to induce buckling, we chose the fundamental thickness mode resonance of our piezoelectric transducer, 6.5 MHz, far below the resonance frequencies of the GVs or the GV agglomerates. Buckling and collapse of the GVs will consequently rely upon intense ultrasound rather than any resonant amplification. With sufficient input power to the transducer, we were able to obtain acoustic pressures of 89 to 400 kPa (*see* Table S1), as calculated via the equation of state and the LDV-measured vibration amplitude on the surface of the acoustic device with $p_a = \rho_s c^2 k\delta$, determining the pressure in the fluid by noting the pressure transmission ratio from the acoustic device to the fluid as $T = \frac{Z_L - Z_w}{Z_L + Z_w} = 0.15$, where $Z_L = 18.5 \times 10^6$ Pa-s/m^3 is the acoustic impedance of LN and $Z_w = 1.5 \times 10^6$ Pa-s/m^3 is the acoustic impedance of water.

The vibration response of the GVs due to the acoustic pressure produced by our transducer at 6.5 MHz is shown in Fig. 3. The vibration amplitude grows from 10 to nearly 100 nm, much larger than the 10–100 pm displacements observed at the GV and agglomerated GV linear resonance frequencies in Figs. 1 and 2, respectively. As the acoustic pressure is increased to between 89 and 132 kPa, the GVs' displacement amplitude grows from 5 to 10 nm (*see* the green area in Fig. 3) with displacement characteristic of large amplitude bubble oscillations in Fig. 3(d), a plot of the real-time response of the GVs. The physical response of a bubble is different in the compression and expansion phases,[37] leading to a periodic response with a change in slope as the bubble transitions between the two phases as observed in these GVs. It is worth noting here that the LDV provides information on the direction of deformation, with positive displacement

here implying motion of the measured surface towards the substrate and away from the LDV system, towards collapse, while negative displacement values are away from the substrate and towards the LDV.

There is a significant increase in the displacement amplitude to around 40 nm as the acoustic pressure reaches 175 kPa (*see* the blue area in Fig. 3), with the GVs' time-based response exhibiting nearly limiting sawtooth oscillations in Fig. 3(e). This vibration amplitude remains constant with an increase in the acoustic pressure to just beyond 320 to 370 kPa, at which point the displacement doubles once again to just over 80 nm (*see* the pink area in Fig. 3)—but only for one to a very few cycles of vibration. As shown in Fig. 3(f), the application of such high acoustic pressure causes large displacements, first towards collapse, then away from the substrate, again towards collapse at a lower amplitude, and finally followed by a much weaker vibration response from the GVs. This indicates irreversible buckling and collapse of the GVs. It is worth noting that the measured vibration amplitude of slightly more than 80 nm roughly corresponds to one-half the size of the GV itself: taking into account the wall thickness of the GV, this could reasonably represent the internal radius of the cavity driven to collapse from the buckling.

We calculated the radiated sound pressure of the GVs $P_{rad} = \rho_l(2R\dot{R}^2 + R^2\ddot{R})/d$ based on the LDV-measured real-time vibration amplitude data of the GVs, $R = R(t)$, where d is the distance of the measurement from the GVs.[32] The fast Fourier-transformed P_{rad} frequency spectra in Fig. 3(g-i) show that the number and intensity of peaks in the spectra grows with an increase in the excitation pressure. As the excitation pressure is increased from (Fig. 3(g)) 132 kPa to 178 and 330 kPa (Fig. 3(h,i), respectively), the appearance of harmonic responses in the emitted GVs' pressure indicates a transition to finite non-sinusoidal deformation of the GVs and participation of these higher frequency modes. The increase in both the number and amplitude of these harmonics with increasing excitation pressure is a strong indicator of building towards collapse of the GVs, as modal participation in an instantaneous change in displacement would extend to very high harmonics with linearly decreasing modal amplitudes. Furthermore, at 330 kPa (Fig. 3(i)), the appearance of resonances not associated with any of the standard linear

responses of the system—a subharmonic response at 3.25 MHz and superharmonic responses at 9.65 and 21.8 MHz—indicate a nonlinear mechanism in the GV response and support the contention that the GVs are buckling and approaching collapse.

The 178 kPa produced from our transducer in our study is between the critical pressure required for buckling according to Cherin, *et al.*,[32] (92.4 kPa) and Lakshmanan, *et al.*[18] (200 kPa), while at higher amplitudes our transducer produces acoustic pressures sufficient to achieve the critical pressure estimates by Lakshmanan, *et al.* The difference between the buckling pressure threshold predicted in Lakshmanan's work and our experiments can be attributed to different buckling observation and pressure measuring methods. Lakshmanan, *et al.* represents the intensity of GVs' vibration with intensity measured in ultrasound scanning images while we performed direct observation of the displacement of the GVs in our study but must compute the resulting pressures. The limited observability of the true GV motion via our LDV may also be a factor in the relatively low prediction of the threshold pressure required to collapse the GVs in our measurements: only motion along the laser is measured via the LDV, though the GV motion is certainly more complex.

Experimental methods and materials

Gas vesicles

The GV used for this study is Anabaena flosaquae (Ana) GV (CCAP 1403/13F, Culture Collection of Algae and Protozoa, Scottish Marine Institute, Oban, UK), produced by a green filamentous cyanobacterium that naturally inhabit freshwater lakes.[13,38] The GVs were purified from these cells as previously described.[38] A standard quality assurance step is taken by measuring the individual diameters of a sample of the GVs before and after their static pressure-driven collapse at 100–1200 kPa. These measurements were carried out using a system composed of an echoVis Vis-NIR light source coupled with an STS-VIS spectrometer (Ocean Optics, Largo, FL USA), and a 176.700-QS sample chamber (Hellma Analytics, College Park, GA USA). Next, the external shell

protein GvpC was removed from the GVs to produce the harmonic GVs used in this study.[38] Finally, the GVs were clustered using sulfo-NHS-biotin (10,000-fold molar excess, Thermo Fisher Scientific, Carlsbad, CA USA) and streptavidin (100-fold molar excess, G-Biosciences, St. Louis, MO USA), facilitating dense GV binding to our LDV setup.[38] Sufficient GVs are present to produce laterally dense agglomerations, and unbound GVs are removed before the experiment. The clustering also enabled sufficient reflection of the 532-nm laser light in our LDV measurements via the setup illustrated in Fig. 1(a-d), producing a low-noise displacement measurement signal. The mean size of the GV clusters was 615.3±24.5 nm, determined with dynamic light scattering measurements (Zetasizer Nano ZS, Malvern Pananalytical, Worcestershire UK). The measured optical density was 11.4. Details of the preparation and handling process may be found in the previous literature.[38] The utility of the GVs in ultrasonic imaging is illustrated via its the signal magnification ability through an agar phantom scan provided in Supplementary Figure S1.

Single-crystal lithium niobate transducer

The 5 mm wide × 8 mm long thickness-mode transducers used as acoustic sources in this study were diced from 500 μm thick, 100 mm diameter, double-side optically polished, 127.86 Y-rotated, X-propagating single-crystal lithium niobate (LN) wafers (Roditi, London, UK) chosen for their superior thickness mode performance as described in detail elsewhere.[39] Electrodes were formed on both faces of the wafer prior to dicing using sputter deposition of 500 nm of gold. The acoustic energy generated by these transducers was in part coupled to the GVs via a thin fluid meniscus through the arrangement shown in Fig. 1(a–d). This was done to minimize both the direct measurement of the transducer's motion by the LDV and the indirect measurement of any possible motion of the fluid meniscus covering the Au-bound GVs that might arise in other arrangements. The transducer was placed at 45° to avoid blocking the LDV laser. An acrylic mounting, omitted for clarity, was used to hold the transducer and LN-gold substrate in place.

LN-gold substrate for streptavidin-biotin binding of the GVs

The gold surface was modified to attach the GV through biotin-avidin bonding as detailed in the literature.[11] The devices were first cleaned through hexane, ethanol, and deionized water, and then finally dried using compressed dry, clean air. The devices were then immersed into a solution contains 0.05 M cystamine dihydrochloride (CA, Sigma Aldrich, St. Louis, MO, USA) and 0.05 M 2-mercaptoethanol (ME, Sigma Aldrich) with DI water as solvent to create sulfur bonds on the gold substrate. After leaving the devices immersed for 24 hr to await completion of the bonds, they were removed and carefully rinsed with deionized water and ethanol before drying them using compressed dry, clean air. The devices were then immersed into a NHS-biotin solution prepared through the reaction of biotin (Sigma Aldrich) mixed with 0.12 mol N,N-diisopropylethylamine (DIPEA, Sigma Aldrich), O-(N-succinimidyl)-N,N,N′,N′-tetramethyluonium (TSTU, Sigma Aldrich, in 10 ml N,N-dimethylformamide (DMF, Sigma Aldrich) solution. At this point, the NHS-biotin bonding on the gold substrate has been established. We then pipetted a 1 mL avidin-GV solution onto the NHS-biotin-gold substrate and waited 30 min to ensure sufficient biotin-avidin bonding on the gold substrate. The devices were subsequently rinsed with deionized water to remove unbound GVs.

Fourier-transform infrared spectroscopy using a liquid nitrogen cooled MCT detector (FTIR, Perkin Elmer, Waltham, MA, USA; additional details in Supplemental Information) was used to confirm NHS-biotin bonding on the gold substrate. Fifty patterns were accumulated at a resolution of 4 cm^{-1} for a single run.

LDV measurements of GV responses to acoustic irradiation

The flat, GV-bonded gold layer was placed perpendicularly to the laser from the LDV; the laser was passed through a 50x lens (M-plan 50x objective, Mitutoyo, Kanagawa Japan) to reduce the depth of coherence (akin to the depth of field) to about 1 μm for observation. A thin layer of deionized water was added onto the surface of the bottom substrate with a fluid bridge to the transducer as a means to couple the acoustic wave from the transducer onto the inert substrate

with GVs bonded to its surface; the gold was mildly hydrophilic in this study, and the fluid bridge was therefore stable. The depth of the water layer was set at 1 to 2 mm, much larger than the wavelength of the acoustic wave, but sufficiently thin to facilitate observation of the GV's surface morphology through LDV. A sinusoidal electric signal from a function generator (SG 380, Stanford Research Systems, Sunnyvale, CA) was used to drive the transducer via a high-frequency amplifier (ZHL–1–2W, Mini-Circuits, Brooklyn, NY, USA) from 9 kHz to 2 GHz. The excitation was non-resonant for a vast majority of this frequency range, but sufficient to drive GV motion observable by the LDV. Near the fundamental thickness-mode resonance at 6.5 MHz of the transducer, the acoustic pressure that could be generated by the transducer was 10 to 400 kPa, sufficient to examine GV collapse according to predictions in the literature.[32,38]

We performed finite-element modal analyses of the GVs (COMSOL Multiphysics 5.4, COMSOL, Burlington, MA USA) to determine the resonance frequencies and modes of a single GV. The elongated GV capsule—or *allantoid*—GV dimensions were 140 nm diameter and 494 to 544 nm total length with a Young's modulus $E = 3$ GPa, Poisson's ratio $\nu = 0.34$ and density $\rho = 1320$ kg/m^3.[31] The thickness of the membrane was modeled as 2 nm based on reports from the literature.[19] A portion of the cylindrical shape along the long edge equivalent to one-eighth of the total surface area was fixed to simulate the strong biotin-avidin bonding between the GV and gold substrate.[40] Based on results from a lumped constant approximation,[41] the effect on the resonance frequencies by damping of water was negligible, allowing us to neglect the effects of surface tension and thermal conductivity.

Acknowledgement

This work was in significant part generously supported by a research grant from the W.M. Keck Foundation. This work was performed in part at the San Diego Nanotechnology Infrastructure (SDNI) of UCSD, a member of the National Nanotechnology Coordinated Infrastructure, supported by the National Science Foundation (Grant ECCS–1542148). The authors wish to express

their gratitude to Eric Lawrence, Jerome Eichenberger, Mario Pineda, and Michael Frech from Polytec for their extraordinary help in this work.

Supporting Information Available

Agar phantom scan

Gas vesicles have strong ultrasound contrast due to the gas encapsulated within them, as indicated with an 18 MHz transducer (L22–14v, Verasonics, Kirkland, WA USA) in Fig. S1(a). Moreover, some gas vesicle variants, such as stripped Ana GVs as the focus of this study, have nonlinear contrast (Fig. S1b). This facilitates the use of amplitude modulation schemes to produce a highly specific map of GV distribution within the imaging plane. If needed, high hydrostatic or ultrasonic pressure can collapse GVs, "erasing" their signals, as performed here with the 18 MHz transducer at 2.09 MPa to produce Fig S1(c).

FTIR Results

The gold substrate is not active in the infrared range of 1400–2400 cm^{-1}, so no reduction in the transmission appears over this range in Suppl. Fig. S2(a). After biotin is bound to the gold with CA and ME as the middle layer, significant reductions in transmission are found as seen in Fig. S2(b). The most obvious peak is at 1680 cm^{-1}, which corresponds to the amide I vibration mode together with the C=O stretch of biotin. This result tells us that the gold substrate is bonded with NHS-biotin.

Exploring the possibility that the GVs are simple bubbles

The importance of the elastic membrane used in the main portion of the text in the modified Rayleigh-Plesset equation is best illustrated by computing the resonance frequencies of a representative bubble that *lacks* this membrane. Using the classic Rayleigh-Laplace equation,

$$f^2 = \frac{\sigma}{R^3}\frac{(j-1)(j+1)(j+2)}{(j+1)\rho^+ + j\rho^-}, \tag{4}$$

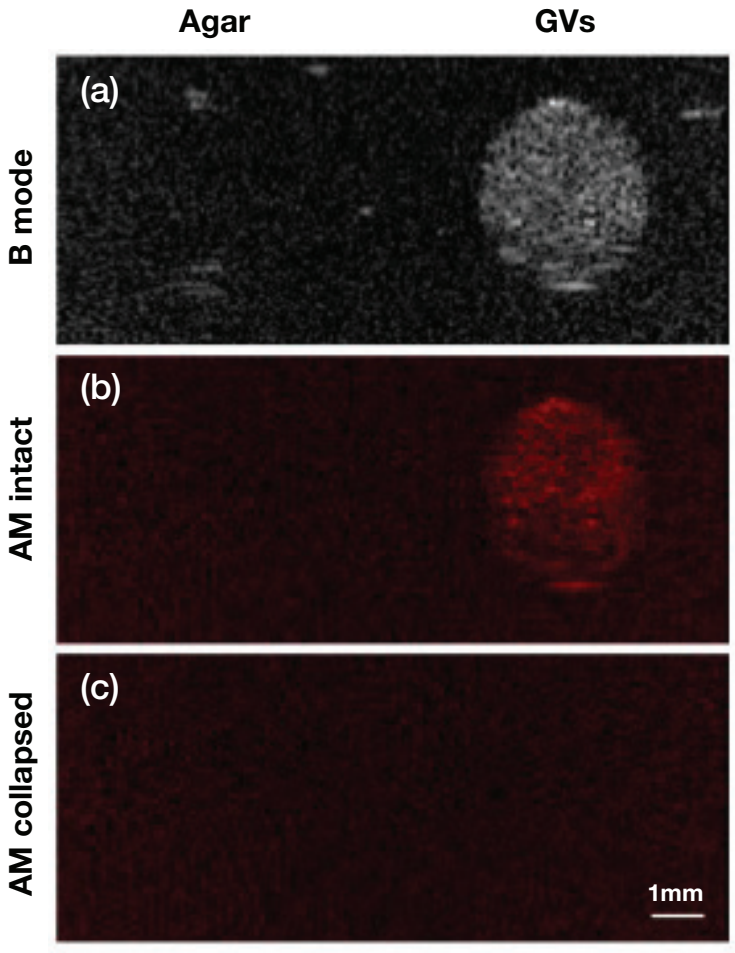

Figure S1: Linear and non-linear ultrasound contrast images of stripped Ana GVs. (a) The linear contrast of GVs can be detected using an anatomic B-mode ultrasound scan at 18 MHz. The result of the scan for an agar-filled well is provided for comparison on the left. (b) The non-linear contrast of stripped Ana GVs can be observed using the amplitude modulation pulse sequence. (c) If necessary, the GVs can be "erased" via apparent collapse using high pressure; in this case 2.09 MPa ultrasound from a commercial transducer.

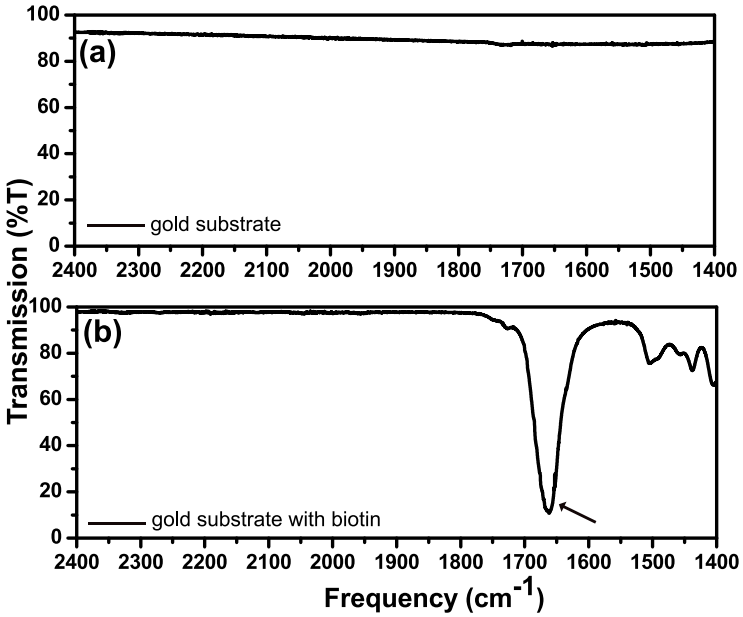

Figure S2: FTIR results indicate that compared to the (a) response of a pure gold substrate prior to before any treatment, (b) biotin produces significant transmission changes after binding it to the gold substrate using CA and ME. The arrow in (b) indicates a characteristic peak at 1680 cm^{-1} associated with the NHS-biotin bond.

with the dimensions and properties chosen to match the GV in a manner similar to the coated bubble calculations, where σ is the protein-air surface tension (0.2 mN/m^2), R is the radius of the bubbles, j is the mode number ($j > 1$), ρ^+ is the density inside the bubbles, and ρ^- is the density outside the bubbles.[42] The fundamental and first harmonic resonance frequencies predicted by this equation are 190 MHz and 301 MHz, substantially less than the corresponding observed experimental results of 1.02 GHz and 1.7 GHz.

Exploring the possibility that the GVs are solid particles

It could be that the GVs are in fact solid nano-sized particles. We consider the resonance frequencies that solid GVs would produce using a classic equation from Lamb.[43] The equation defines the fundamental resonance frequency of a solid sphere f_{solid} through the relationship $\frac{f_{\text{solid}}^2 \rho}{Y} R^2/(4\pi^3) \approx 1.8$. Treating the allantoid shape as approaximately spheriod, and equating the volume, the radius of an equivalent sphere is $R = 1.3 \times 10^{-7}$ m, and $\rho \sim 10^3$ kg/m^3 and

$Y \sim 3$ GPa[13] are the density and rigidity, the lowest possible resonance frequency is on the order of 10^{11} Hz. The high Young's modulus comes from the protein layer. The resonance frequency from this calculation shows that it is two orders of magnitude greater than our observations, suggesting that GVs are not solid particles.

Mode shapes of surface-bound and free GVs of different lengths

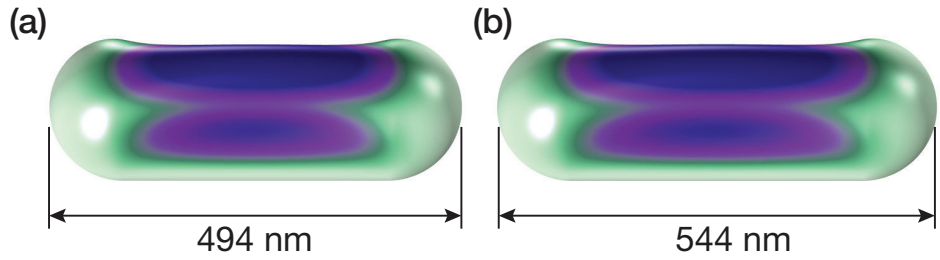

Figure S3: The computed mode shapes of a surface-bound GV, with one-eighth of the cylindrical portion of the GV nearest the bottom fixed in place, representing binding to a surface. The length of the GV is different (a) 494 nm and (b) 544 nm with resonance frequency at 1.092 GHz and 1.088 GHz, respectively, within 4.3% of the experimentally measured fundamental resonance frequency at 1.047 GHz.

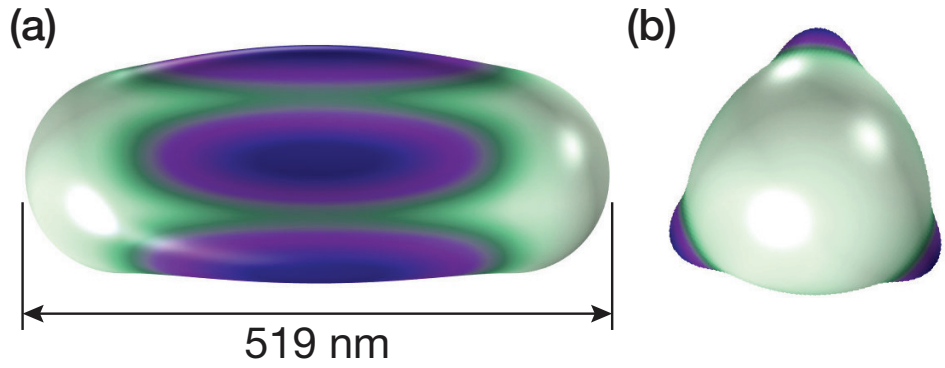

Figure S4: A GV completely free to move produces a computed fundamental resonance frequency of 0.992 GHz, remarkably only 6.8% less than the experimentally measured fundamental resonance frequency of 1.047 GHz for bound and agglomerated GVs.

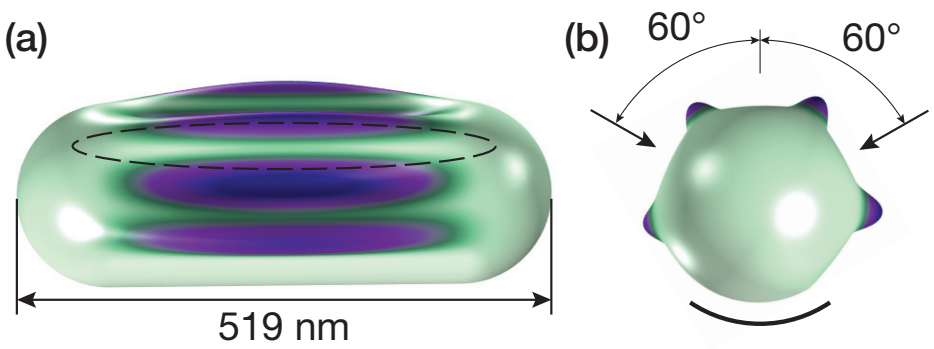

Figure S5: The computed mode shapes of a surface-bound GV; with it bound with other GVs at 60° from the vertical via symmetry boundary conditions. The boundary conditions are applied along lines defined upon the GV's cylindrical portion, one shown and one hidden upon the back side of this GV; and one-eighth of the cylindrical portion of the GV nearest the bottom fixed in place as indicated with the heavy curved line in the end view. Each symmetry-bound agglomeration line lies 45° from the vertical and is along the cylindrical portion of the allantoid shape. The fundamental resonance frequency produced by this object is 1.06 GHz, 1.2% above the 1.047 GHz resonance found for the GVs in our experiments.

Resonance response of GVs at 300 MHz depends upon GV agglomerate size

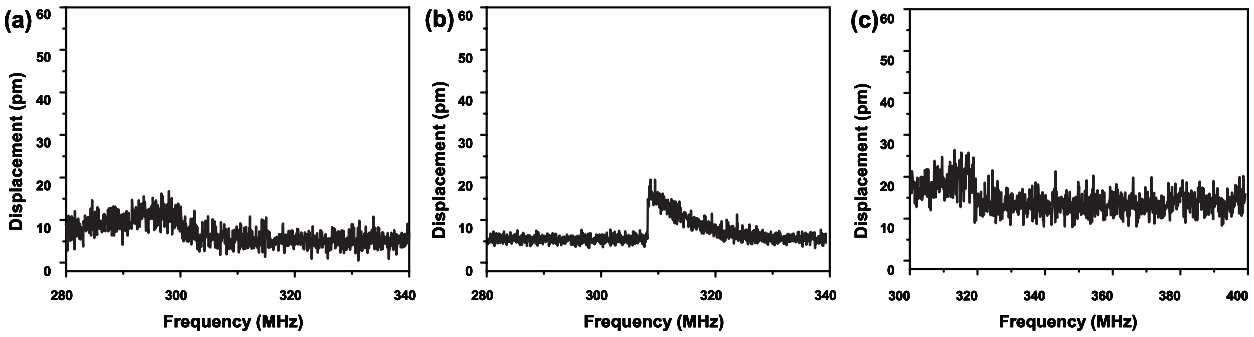

Figure S6: Resonances observed via the LDV at (a) close to 295 MHz, (b) close to 310 MHz, and (c) close to 310 MHz around appear to arise from the vibration of GV agglomerations of around 615 nm in size (*see* main text for details).

The measured transducer output vibration amplitude and pressure as dependent upon the input power

Table S1: The measured amplitude of vibration upon the transducer and the calculated acoustic pressure in the fluid adjacent the transducer, depending upon the power input into our transducer

Input power (W)	Displacement (nm)	Calculated acoustic pressure (kPa)
1	0.700	89
2	1.04	132
3	1.4	178
4	1.67	212
5	1.9	242
6	2.6	330
7	2.8	356

References

(1) Ferrara, K.; Pollard, R.; Borden, M. Ultrasound Microbubble Contrast Agents: Fundamentals and Application to Gene and Drug Delivery. *Annu. Rev. Biomed. Eng.* **2007**, *9*, 415–447.

(2) Stride, E.; Saffari, N. Microbubble ultrasound contrast agents: a review. *Proceedings of the Institution of Mechanical Engineers, Part H: Journal of Engineering in Medicine* **2003**, *217*, 429–447.

(3) Agarwal, A.; Ng, W. J.; Liu, Y. Principle and applications of microbubble and nanobubble technology for water treatment. *Chemosphere* **2011**, *84*, 1175–1180.

(4) Liang, H.-D.; Noble, J. A.; Wells, P. N. Recent Advances in Biomedical Ultrasonic Imaging Techniques. *Interface Focus* **2011**, 475–476.

(5) Snipstad, S.; Sulheim, E.; de Lange Davies, C.; Moonen, C.; Storm, G.; Kiessling, F;

Schmid, R.; Lammers, T. Sonopermeation to improve drug delivery to tumors: from fundamental understanding to clinical translation. *Expert Opinion on Drug Delivery* **2018**,

(6) Cai, W. B.; Yang, H. L.; Zhang, J.; Yin, J. K.; Yang, Y. L.; Yuan, L. J.; Zhang, L.; Duan, Y. Y. The optimized fabrication of nanobubbles as ultrasound contrast agents for tumor imaging. *Scientific Reports* **2015**, *5*, 13725.

(7) Yin, T.; Wang, P.; Zheng, R.; Zheng, B.; Cheng, D.; Zhang, X.; Shuai, X. Nanobubbles for enhanced ultrasound imaging of tumors. *International Journal of Nanomedicine* **2012**, *7*, 895.

(8) De Jong, N.; Bouakaz, A.; Frinking, P. Basic acoustic properties of microbubbles. *Echocardiography* **2002**, *19*, 229–240.

(9) Kim, T.-H.; Kim, H.-Y. Disruptive bubble behaviour leading to microstructure damage in an ultrasonic field. *Journal of Fluid Mechanics* **2014**, *750*, 355–371.

(10) Shapiro, M. G.; Goodwill, P. W.; Neogy, A.; Yin, M.; Foster, F. S.; Schaffer, D. V.; Conolly, S. M. Biogenic gas nanostructures as ultrasonic molecular reporters. *Nature Nanotechnology* **2014**, *9*, 311–316.

(11) Yam, C.-M.; Pradier, C.-M.; Salmain, M.; Marcus, P.; Jaouen, G. Binding of biotin to gold surfaces functionalized by self-assembled monolayers of cystamine and cysteamine: Combined FT-IRRAS and XPS characterization. *Journal of Colloid and Interface Science* **2001**, *235*, 183–189.

(12) Lu, G. J.; Farhadi, A.; Mukherjee, A.; Shapiro, M. G. Proteins, air and water: reporter genes for ultrasound and magnetic resonance imaging. *Current Opinion in Chemical Biology* **2018**, *45*, 57–63.

(13) Walsby, A. E. Gas vesicles. *Microbiological Reviews* **1994**, *58*, 94–144.

(14) Lu, G. J.; Farhadi, A.; Szablowski, J. O.; Lee-Gosselin, A.; Barnes, S. R.; Lakshmanan, A.; Bourdeau, R. W.; Shapiro, M. G. Acoustically modulated magnetic resonance imaging of gas-filled protein nanostructures. *Nature Materials* **2018**, *17*, 456.

(15) Farhadi, A.; Ho, G. H.; Sawyer, D. P.; Bourdeau, R. W.; Shapiro, M. G. Ultrasound Imaging of Gene Expression in Mammalian Cells. *bioRxiv* **2019**, 580647.

(16) Szablowski, J. O.; Bar-Zion, A.; Shapiro, M. G. Achieving Spatial and Molecular Specificity with Ultrasound-Targeted Biomolecular Nanotherapeutics. *Accounts of chemical research* **2019**, *52*, 2427–2434.

(17) Bourdeau, R. W.; Lee-Gosselin, A.; Lakshmanan, A.; Farhadi, A.; Kumar, S. R.; Nety, S. P.; Shapiro, M. G. Acoustic reporter genes for noninvasive imaging of microorganisms in mammalian hosts. *Nature* **2018**, *553*, 86.

(18) Lakshmanan, A.; Farhadi, A.; Nety, S. P.; Lee-Gosselin, A.; Bourdeau, R. W.; Maresca, D.; Shapiro, M. G. Molecular engineering of acoustic protein nanostructures. *ACS Nano* **2016**, *10*, 7314–7322.

(19) Maresca, D.; Lakshmanan, A.; Abedi, M.; Bar-Zion, A.; Farhadi, A.; Lu, G. J.; Szablowski, J. O.; Wu, D.; Yoo, S.; Shapiro, M. G. Biomolecular Ultrasound and Sonogenetics. *Annual Review of Chemical and Biomolecular Engineering* **2018**, *9*, 229–252.

(20) Pitt, W. G.; Husseini, G. A.; Staples, B. J. Ultrasonic drug delivery–a general review. *Expert Opinion on Drug Delivery* **2004**, *1*, 37–56.

(21) Dayton, P. A.; Morgan, K. E.; Klibanov, A. L.; Brandenburger, G. H.; Ferrara, K. W. Optical and acoustical observations of the effects of ultrasound on contrast agents. *IEEE Transactions on Ultrasonics, Ferroelectrics, and Frequency Control* **1999**, *46*, 220–232.

(22) Bouakaz, A.; Versluis, M.; de Jong, N. High-speed optical observations of contrast agent destruction. *Ultrasound in Medicine and Biology* **2005**, *31*, 391–399.

(23) Versluis, M. High-speed imaging in fluids. *Experiments in Fluids* **2013**, *54*, 1458.

(24) Sijl, J.; Gaud, E.; Frinking, P. J.; Arditi, M.; de Jong, N.; Lohse, D.; Versluis, M. Acoustic characterization of single ultrasound contrast agent microbubbles. *The Journal of the Acoustical Society of America* **2008**, *124*, 4091–4097.

(25) Leighton, T.; Ramble, D.; Phelps, A.; Morfey, C.; Harris, P. Acoustic detection of gas bubbles in a pipe. *Acta Acustica United with Acustica* **1998**, *84*, 801–814.

(26) Koyama, D.; Kotera, H.; Kitazawa, N.; Yoshida, K.; Nakamura, K.; Watanabe, Y. Vibration of a single microcapsule with a hard plastic shell in an acoustic standing wave field. *IEEE Transactions on Ultrasonics, Ferroelectrics, and Frequency Control* **2011**, *58*, 737–743.

(27) Kotera, H.; Koyama, D.; Kitazawa, N.; Yoshida, K.; Nakamura, K.; Watanabe, Y. A Simultaneous Observation System for Microbubble Vibration in an Acoustic Field by using a High-speed Camera and an LDV. *Proc. ICA 2010* **2010**, 23.

(28) Maresca, D.; Lakshmanan, A.; Lee-Gosselin, A.; Melis, J. M.; Ni, Y.-L.; Bourdeau, R. W.; Kochmann, D. M.; Shapiro, M. G. Nonlinear ultrasound imaging of nanoscale acoustic biomolecules. *Applied Physics Letters* **2017**, *110*, 073704.

(29) Connacher, W.; Zhang, N.; Huang, A.; Mei, J.; Zhang, S.; Gopesh, T.; Friend, J. Micro/nano acoustofluidics: materials, phenomena, design, devices, and applications. *Lab on a Chip* **2018**, *18*, 1952–1996.

(30) Sader, J. E.; Yousefi, M.; Friend, J. R. Uncertainty in least-squares fits to the thermal noise spectra of nanomechanical resonators with applications to the atomic force microscope. *Review of Scientific Instruments* **2014**, *85*, 025104.

(31) Marmottant, P.; van der Meer, S.; Emmer, M.; Versluis, M.; de Jong, N.; Hilgenfeldt, S.; Lohse, D. A model for large amplitude oscillations of coated bubbles accounting for buckling and rupture. *The Journal of the Acoustical Society of America* **2005**, *118*, 3499–3505.

(32) Cherin, E.; Melis, J. M.; Bourdeau, R. W.; Yin, M.; Kochmann, D. M.; Foster, F. S.; Shapiro, M. G. Acoustic behavior of Halobacterium salinarum gas vesicles in the high-frequency range: experiments and modeling. *Ultrasound in Medicine and Biology* **2017**, *43*, 1016–1030.

(33) Devin Jr, C. Survey of thermal, radiation, and viscous damping of pulsating air bubbles in water. *The Journal of the Acoustical Society of America* **1959**, *31*, 1654–1667.

(34) McDaniel, J. G.; Akhatov, I.; Holt, R. G. Inviscid dynamics of a wet foam drop with monodisperse bubble size distribution. *Physics of Fluids* **2002**, *14*, 1886–1894.

(35) Plesset, M. S.; Prosperetti, A. Bubble dynamics and cavitation. *Annual Review of Fluid Mechanics* **1977**, *9*, 145–185.

(36) Rayleigh, L. VIII. On the pressure developed in a liquid during the collapse of a spherical cavity. *The London, Edinburgh, and Dublin Philosophical Magazine and Journal of Science* **1917**, *34*, 94–98.

(37) Marmottant, P.; Bouakaz, A.; Jong, N. d.; Quilliet, C. Buckling resistance of solid shell bubbles under ultrasound. *The Journal of the Acoustical Society of America* **2011**, *129*, 1231–1239.

(38) Lakshmanan, A.; Lu, G. J.; Farhadi, A.; Nety, S. P.; Kunth, M.; Lee-Gosselin, A.; Maresca, D.; Bourdeau, R. W.; Yin, M.; Yan, J. Preparation of biogenic gas vesicle nanostructures for use as contrast agents for ultrasound and MRI. *Nature protocols* **2017**, *12*, 2050–2080.

(39) Collignon, S.; Manor, O.; Friend, J. Improving and Predicting Fluid Atomization via Hysteresis-Free Thickness Vibration of Lithium Niobate. *Advanced Functional Materials* **2018**, *28*, 1704359.

(40) Weber, P.; Ohlendorf, D.; Wendoloski, J.; Salemme, F. Structural origins of high-affinity biotin binding to streptavidin. *Science* **1989**, *243*, 85–88.

(41) Medwin, H. Counting bubbles acoustically: a review. *Ultrasonics* **1977**, *15*, 7–13.

(42) Van der Meer, F. D.; De Jong, S. M. *Imaging Spectrometry: Basic Principles and Prospective Applications*; Springer Science and Business Media, 2011; Vol. 4.

(43) Lamb, H. On the vibrations of an elastic sphere. *Proceedings of the London Mathematical Society* **1881**, *1*, 189–212.